Liquid-phase Hydrodeoxygenation of 4-Propylphenol to Propylbenzene: Reducible Supports for Pt Catalysts

Eveliina Mäkelä[+],*[a] José Luis González Escobedo[+],[a] Jouni Neuvonen,[a] Jouko Lahtinen,[b] Marina Lindblad,[c] Ulla Lassi,[d] Reetta Karinen,[a] and Riikka L. Puurunen[a]

Pyrolysis and liquefaction biocrudes obtained from lignocellulose are rich in phenolic compounds that can be converted to renewable aromatics. In this study, Pt catalysts on reducible metal oxide supports (Nb_2O_5, TiO_2), along with irreducible ZrO_2 as a reference, were investigated in the liquid-phase hydrodeoxygenation (HDO) of 4-propylphenol (350 °C, 20 bar H_2, organic solvent). The most active catalyst was Pt/Nb_2O_5, which led to the molar propylbenzene selectivity of 77%, and a yield of 75% (98% conversion). Reducible metal oxide supports provided an increased activity and selectivity to the aromatic product compared to ZrO_2, and the obtained results are among the best reported in liquid-phase. The reusability of the spent catalysts was also studied. The spent Pt/Nb_2O_5 catalyst provided the lowest conversion, while the product distribution of the spent Pt/ZrO_2 catalyst changed towards oxygenates. The results highlight the potential of pyrolysis or liquefaction biocrudes as a source of aromatic chemicals.

Introduction

The ongoing challenges of climate change and the diminishing reserves of fossil resources call for developing alternative solutions,[1] such as renewable fuels and chemicals.[2] Lignocellulosic biomass is considered a cheap and abundant raw material for bio-based fuels and chemicals, although its recalcitrance and oxygen content hinder its use.[3,4] Pyrolysis and liquefaction are promising technologies for upgrading the whole lignocellulose in a single stream, including the lignin fraction. On the one hand, pyrolysis has been identified as one of the most cost-effective routes compared to gasification and biochemical pathways.[5] On the other hand, liquefaction, in which lignocellulose is depolymerized and partially deoxygenated in a liquid solvent,[6] is suitable for process integration and novel process intensification techniques.[7] However, pyrolysis and liquefaction produce complex liquids, which are unsuitable as fuels and further upgrading processes are necessary. Currently, the most common upgrading process is hydrotreatment.[8,9] Hydrotreatment leads to the removal of oxygen as water[10] and is typically conducted with sulfided NiMo and CoMo catalysts supported on alumina.[9]

Pyrolysis liquids typically contain 15% to 30% water[11] and are chemically unstable and corrosive.[11,12] They are mixtures of hundreds of components, including water, simple oxygenates (e.g. acids, alcohols, ketones and esters), furans, sugars, hydrocarbons, and phenolic compounds.[11,12] Liquefaction biocrudes are similar to pyrolysis liquids, but they are richer in phenolics.[6] Phenols are especially challenging to upgrade due to the strength of the hydroxyl-aryl bond.[12] The hydrodeoxygenation (HDO) of phenols can proceed through any of at least three distinct routes; hydrogenation-dehydration (HYD), direct deoxygenation (DDO), and tautomerization (TAU), as presented in Scheme 1.[13–17]

Since sulfided catalysts require a continuous source of sulfur to maintain their activity,[9] a sulfiding agent needs to be added to the originally low-sulfur feedstock.[16] Hence, alternatives to sulfided catalysts are desirable. Recently, the HDO of phenolics has been studied extensively to produce aromatics with base metal[18–20] or noble metal[14,15,21–24] catalysts. Cyclohexane and other non-aromatics have also been obtained with base[16,25] and noble[15,22,23,26–28] metal catalysts. Product selectivities and reaction rates can be strongly influenced by the solvent and the phase distribution of the components in the reaction mixture.[29–31] Most publications have focused on vapor-phase HDO to obtain aromatics,[14,15,24,27,28,32–37] perhaps targeting process integration with pyrolysis.[37] Works on liquid-phase HDO have aimed at cyclic aliphatics[16] or, in the case of aqueous

[a] E. Mäkelä,[+] J. L. González Escobedo,[+] J. Neuvonen, Dr. R. Karinen, Prof. R. L. Puurunen
Department of Chemical and Metallurgical Engineering
Aalto University School of Chemical Engineering
P.O. Box 16100
00076 AALTO (Finland)
E-mail: eveliina.makela@aalto.fi
[b] Dr. J. Lahtinen
Department of Applied Physics
Aalto University School of Science
P.O. Box 15100
00076 AALTO (Finland)
[c] Dr. M. Lindblad
Neste Corporation
P.O. Box 310
06101 Porvoo (Finland)
[d] Prof. U. Lassi
Research unit of Sustainable Chemistry
University of Oulu
P.O. Box 8000
90014 Oulu (Finland)
[+] These authors contributed equally.

Supporting information for this article is available on the WWW under https://doi.org/10.1002/cctc.202000429

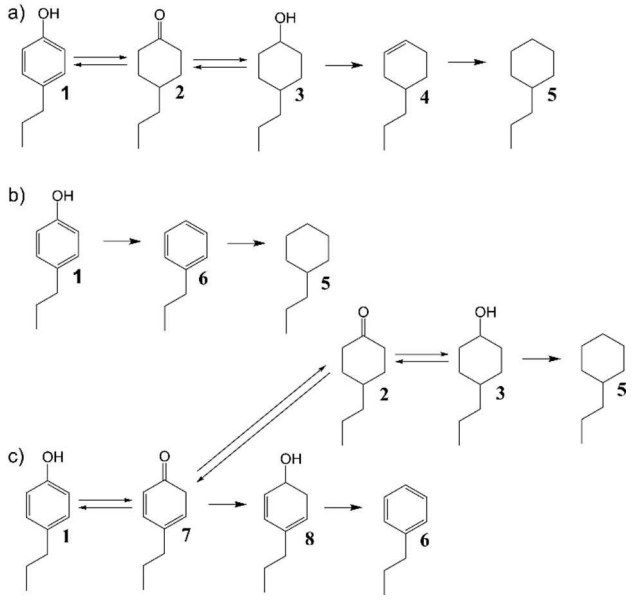

Scheme 1. Proposed pathways[13–17] for 4-propylphenol HDO through a) hydrogenation-dehydration (HYD), b) direct deoxygenation (DDO) and c) tautomerization (TAU) routes. Compounds indicated: **1** 4-propylphenol, **2** 4-propylcyclohexanone, **3** 4-propylcyclohexanol, **5** propylcyclohexane, **6** propylbenzene, **7** 2,4-cyclohexadienone, **8** 2,4-cyclohexadienol.

systems, at aromatics.[19,21,26,38] Unfortunately, water has been found in some cases to cause severe catalyst deactivation by leading to an excessive coverage of the noble metal by oxide species from the support.[21] Concerning the use of non-polar organic solvents in liquid-phase HDO, some studies on alkylphenols to aromatic products have been conducted with MoO_x and Ru-based catalysts.[18,20,39,40] Furthermore, guaiacol HDO in such solvents has been studied extensively with sulfides and noble metal catalysts.[31,41–44] Hellinger et al.[31] compared the influence of non-polar and oxygenated solvents on guaiacol HDO and found that the alkane solvents promoted high conversion and deoxygenation, as well as low sintering of Pt particles. Supported Pt catalysts have been studied for the HDO of alkylphenols to obtain aromatics in vapor-phase[15,24,28,33] and to some extent in aqueous-phase[21] and in liquid alkane solvents.[45] Liquid-phase HDO with an organic solvent might be advantageous for process integration with biomass liquefaction or solvolysis.[6,7] In general, aromatic products are interesting as potential jet fuel components.[46] Additionally, lignin-derived aromatics could also be an important source of industrial chemicals, pharmaceuticals and polymers.[47]

Supported metal catalysts with reducible or irreducible supports have been compared in phenolics HDO. It has been found that reducible metal oxide supports, such as titania and niobia, enhance the deoxygenation activity of noble metal catalysts and result in a high selectivity to aromatics.[14,15,36,48] In the literature, oxygen vacancies[49,50] and strong metal-support-interaction (SMSI)[14,51,52] have been proposed to account for the improved catalytic activity observed with reducible supports. Oxygen vacancies are formed when an oxygen atom is missing from the oxide's crystalline bulk or surface structure (typically created via reduction or via doping with an aliovalent metal oxide, viz. one having a lower oxidation state).[53,54] For example, Schimming et al.[50] found a linear correlation between the number of oxygen vacancies and the activity of ceria-zirconia based catalysts in guaiacol HDO. Regarding SMSI, it promotes HDO, as the active metal is partially covered with e.g. NbO_x or TiO_x species, thus the bare metal sites provide dissociated hydrogen while the oxide sites activate the phenolic oxygen.[51] In this respect, Barrios et al.[14] concluded that the favorable aromatic selectivity of their niobia catalyst was due to oxophilic Nb^{5+} and Nb^{4+} sites interacting with the phenolic oxygen.[14] Chen and Pacchioni[55] concluded that on a Ru/TiO_2 catalyst, the TiO_2 surface reduction with hydrogen caused the formation of Ti^{3+}, which favored the direct deoxygenation of phenol. In view of this background, reducible supports were selected for the present study.

The goal of this study was to investigate the liquid-phase HDO of 4-propylphenol using an organic solvent and reducible metal oxide supports for Pt catalysts to produce propylbenzene. The studied model compound, having a propyl sidechain, was suitable to determine whether sidechain cracking would occur during the reaction. The comparison of reducible supports with each other, such as Nb_2O_5 and TiO_2, in the liquid-phase HDO of phenolics to aromatics has not been reported before. Monoclinic zirconia, an irreducible support,[53] was studied for reference.

Results and Discussion

Catalyst Characterization

X-ray fluorescence

The Pt loadings of the prepared catalysts were estimated with X-ray fluorescence (XRF) and the results are presented in Table 1. The Pt loadings were approximately 3 wt.% for the fresh catalysts and close to 2 wt.% for the spent catalysts, which could indicate that the leaching of the metal occurred within batch residence times of 4 to 5 $g_{cat}\,min\,g_{reactant}^{-1}$ corresponding to reaction times between 34–47 min. For the spent catalyst, the Pt loading was corrected with the produced coke [from thermogravimetric analysis (TGA)], which increased the spent catalysts Pt loading by maximum of 0.1 percentage units.

Physisorption measurements

Physisorption isotherms of the Pt catalysts and the supports, and the corresponding pore size distributions, are presented in Figure S1 in the Supplementary Material. The calculated Brunauer-Emmett-Teller (BET) surface areas, pore volumes, and mean pore diameters (from physisorption) are presented in Table 1. The Pt/TiO_2 and the TiO_2 support presented a Type H3 hysteresis loop (Figure S1c), and the Pt/ZrO_2 and the ZrO_2 support, a Type H1 hysteresis loop (Figure S1e, typical for mesoporous materials with a narrow range of pore sizes), based

Table 1. Properties of fresh and spent Pt catalysts and supports obtained via XRF, physisorption and chemisorption and from STEM images.

Catalyst	N_2 physisorption			CO chemisorption at 25 °C[d]			STEM	
	S_{BET}[a] [$m^2 g^{-1}$]	Pore volume[b] [$cm^3 g^{-1}$]	Average pore diameter[b] [nm]	Irreversible adsorption capacity [$\mu mol_{gas} g_{cat}^{-1}$]	Dispersion	Average particle size [nm]	Average particle size [nm]	Standard deviation of particle size nm]
Nb_2O_5	74	0.12	6.9	n.d.	n.d.	n.d.	n.d.	n.d.
TiO_2	125	0.25	8.6	n.d.	n.d.	n.d.	n.d.	n.d.
ZrO_2	67	0.18	13	n.d.	n.d.	n.d.	n.d.	n.d.
3.1% Pt/Nb_2O_5	85	0.10	5.3	63.4	41%	2.5	1.4	0.3
3.2% Pt/TiO_2	119	0.22	8.5	106.5	69%	1.5	1.3	0.5
2.7% Pt/ZrO_2	80	0.19	12	87.1	57%	1.8	1.9	0.4
2.2% Pt/Nb_2O_5 spent[c]	61	0.10	6.5	13.5	13%	7.8	2.7	1.2
2.5% Pt/TiO_2 spent[c]	69	0.16	12	49.5	48%	2.1	2.1	0.8
1.8% Pt/ZrO_2 spent[c]	68	0.19	11	23.4	23%	4.6	2.9	0.9

[a] Calculated via BET method from 0.05 to 0.3 p/p^0, [b] Calculated via BJH method using adsorption data from 0.2 to 0.9 p/p^0, [c] Catalysts spent in experiments with $\tau_B = 4$ to 5 g_{cat} min greactant^{-1} and washed with EtOH and dried at 100 °C prior to analysis, [d] Prior to chemisorption measurements, samples were reduced at 290 °C. Note that the spent catalysts Pt loading was corrected by the produced coke, and the corrected values were used for Pt dispersion and particle size calculations from chemisorption measurements.

on the IUPAC classification;[56] whereas, the isotherms of Pt/Nb_2O_5 and Nb_2O_5 showed a double hysteresis loop (Figure S1a). Similar isotherms and the evolving of the Nb_2O_5 morphology with increasing calcination temperature has been reported elsewhere.[57] The pore size distributions of all the catalysts were calculated from the adsorption branches to avoid an artifact at ca. 4 nm caused by cavitation.[58] Of the used supports, the highest calculated specific surface area was for the TiO_2 support, whereas ZrO_2 and Nb_2O_5 had similar surface areas. Compared to the other supports, the Nb_2O_5 support had a lower pore volume and the ZrO_2 support a larger mean pore diameter. The pore volumes decreased slightly after impregnating Pt on Nb_2O_5 and TiO_2. The surface areas of Pt/ZrO_2 and Pt/Nb_2O_5 increased and the surface area of Pt/TiO_2 decreased compared to the supports. All the mean pore diameters decreased slightly after the impregnation of the Pt metal.

Chemisorption measurements and STEM particle sizes

Table 1 contains the metal dispersion calculated from CO chemisorption (25 °C) isotherms, as well as the particle sizes calculated from the chemisorption measurements and estimated from the scanning transmission electron microscopy (STEM) images. The chemisorption isotherms measured for the fresh and spent catalysts are presented in Figure S2 of the Supplementary Material, and the STEM images are presented in Figure 1. The highest Pt dispersion (69%) was obtained on the TiO_2 support and the lowest (41%) on Nb_2O_5. The particle sizes for Pt on TiO_2 (ca. 1.4 nm) and on ZrO_2 (ca. 1.9 nm) supports were similar with both methods (chemisorption and STEM), but for Pt/Nb_2O_5, the chemisorption particle size (2.5 nm) was higher compared to the average particle size measured from the STEM images (1.4 nm). This might be due to the SMSI causing the partially reduced support species to cover the metal and decrease its availability for chemisorption[59] or due to incorrect assumption of CO:metal adsorption stoichiometry

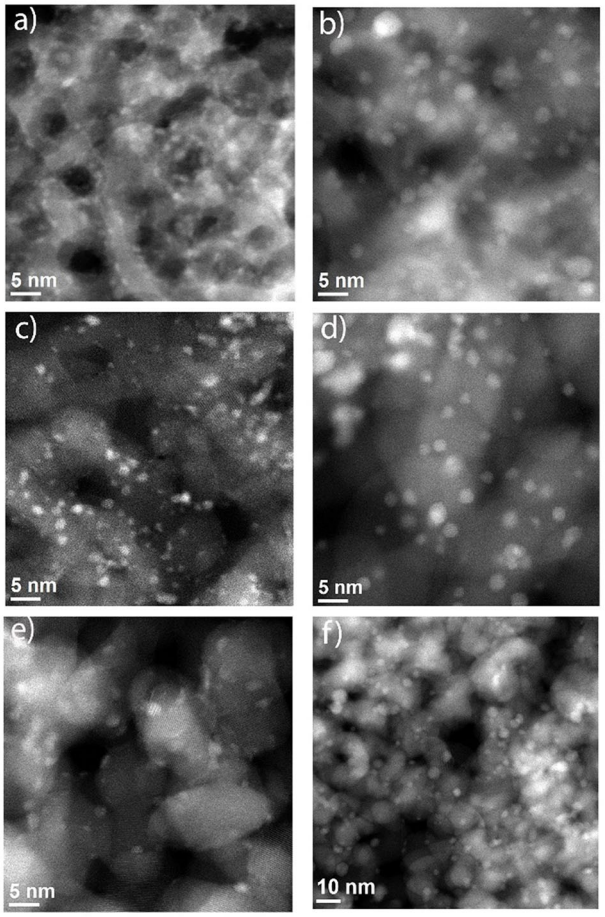

Figure 1. Dark-field STEM images of the fresh and spent catalysts: a) Pt/Nb_2O_5, b) spent Pt/Nb_2O_5, c) Pt/TiO_2, d) spent Pt/TiO_2, e) Pt/ZrO_2 and f) spent Pt/ZrO_2. Note that the Pt particles are seen as lighter dots. Note the difference in scale.

of 1.[60] However, as listed elsewhere,[60] 1 is a widely used approximation for CO adsorption stoichiometry on noble

metals. Pt particle size distribution histograms (from STEM images) for the fresh and spent catalysts are presented in Figure 2.

X-ray diffraction

X-ray diffractograms for the supports, fresh catalysts, and spent catalysts are shown in Figure S3. The Nb_2O_5 support calcined at 500 °C presented pseudo-hexagonal Nb_2O_5 TT phase.[57,61] The TiO_2 support presented anatase and the ZrO_2 support monoclinic phase. The diffractograms of the prepared catalysts were similar to those of their bare supports, and no diffraction peaks for Pt were detected in any of the fresh catalysts, which might indicate small metal particles and high Pt metal dispersion.

X-ray photoelectron spectroscopy

The wide X-ray photoelectron spectra for the Pt/Nb_2O_5, Pt/TiO_2 and Pt/ZrO_2 catalysts are presented in Figures S4, S5 and S6, respectively. The support materials showed main peaks at binding energies (BE) 182.0 eV for $Zr3d_{5/2}$, 207.5 eV for $Nb3d_{5/2}$, and 458.7 eV for $Ti2p_{3/2}$ corresponding to ZrO_2, Nb_2O_5, and TiO_2 (Figure S7), respectively.[62] The presence of other oxidation states [for example niobium has five oxidation stages (+5 to −1), three of which can exist as oxides (Nb_2O_5, NbO_2, and NbO)[63]] on the supports' surfaces cannot be ruled out, but their relative amounts were beyond the detection limit. The Pt4f region in Figure 3 indicates the presence of at least two chemical states of Pt in each catalyst. Deconvolution with three doublets corresponding to metallic Pt (71.2 eV), $Pt(OH)_2$ (72.6 eV), and PtO_2 (74.8 eV)[62] with fixed peak positions were applied to all three spectra. The number of free parameters was kept as small as possible. The intensity ratio of the $4f_{7/2}$ and $4f_{5/2}$ peaks was fixed to 4:3, their separation to 3.33 eV and the peak widths of the doublet components were kept equal. The result of the deconvolution was reasonable and suggests the presence of Pt^{2+} in $Pt(OH)_2$ and Pt^{4+} in PtO_2 on zirconia (70%/30%) and on niobia (50%/50%) surfaces, whereas Pt^0 and Pt^{2+} in $Pt(OH)_2$ existed on titania (50%/50%).

Temperature programmed desorption

The catalysts' acidity and basicity were studied with NH_3 and CO_2 temperature programmed desorption (TPD), respectively. The calculated total acidity and basicity for the fresh catalysts are presented in Table 2, and the corresponding TPD profiles are shown in Figure S8 of the Supplementary Material. In our measurements, the total acidity for 3 wt.% Pt/Nb_2O_5 catalysts was 995 μmol/g catalyst. The total acidity was the lowest for Nb_2O_5 supported catalyst and the highest for the TiO_2 supported catalyst. Hydrated niobium oxide, also referred to as niobic acid, is known to have a high acid strength, but the acidic nature disappears when heating above 527 °C.[63] Niobia is known to have both Lewis and Brønsted acid sites; the amount of Lewis acid sites are increasing with pretreatment temperature up to 500 °C and the Brønsted acid sites have a maximum after a thermal treatment at 100 °C.[63] In the NH_3 TPD profiles for Pd/Nb_2O_5 catalyst reduced at 300 and 500 °C by Barrios et al.,[14] a broad peak appeared between 150 °C and 500 °C, whereas we observed continuous removal of NH_3 rather than a peak. Moreover, a clear low temperature CO_2-TPD peak was observed with Nb_2O_5 and Pt/Nb_2O_5 at 100–200 °C indicating weak basic sites.[64] For TiO_2 and ZrO_2, the addition of Pt increased catalyst acidity, but with Nb_2O_5, the acidity decreased after Pt impregnation. No significant differences were observed in the total basicity for the catalysts and supports.

Table 2. The concentrations of acid and basic sites determined for the calcined and reduced fresh supports and catalysts from NH_3–TPD or CO_2–TPD, respectively.

Catalyst	Total acidity [mmol g^{-1}]	Total basicity [mmol g^{-1}]
Nb_2O_5	1.2	0.2
TiO_2	0.5	0.2
ZrO_2	1.0	0.3
Pt/Nb_2O_5	1.0	0.2
Pt/TiO_2	2.0	0.2
Pt/ZrO_2	1.5	0.3

Temperature programmed reduction

As Nb_2O_5 and TiO_2 are known to be reducible oxides,[65] temperature programmed reduction (TPR) measurements (Figure 4) were performed to guide the selection of the reduction temperatures for the catalysts. With all the catalysts, small peaks below 150 °C could be attributed to the reduction of Pt.[66] Based on the XPS measurements, metallic Pt was only present on the TiO_2 support and the Pt reduction peak in TPR was perhaps the smallest with TiO_2 support, although not very clearly, which supports the XPS analysis. Aranda et al.[66] studied TPR of Pt on Nb_2O_5 with different Pt loadings (0.5 to 2 wt.%). They noticed a peak between 70 to 90 °C that was assigned to the reduction of superficial α-PtO_2 species. With higher Pt loading (> 0.8 wt.%), they also had a peak at RT that was assigned to the reduction of bulk PtO_2 having low interaction with the support.[66]

In our study, no peaks associated to ZrO_2 reduction were noticed. With the reducible supports (Nb_2O_5 and TiO_2), peaks attributed to support reduction were visible at 400 to 550 °C for TiO_2 and from 400 °C onwards for Nb_2O_5. Adding Pt to the supports shifted the reduction of the supports to lower temperature in both cases (Nb_2O_5 and TiO_2), which can be associated to metal assisted reduction of the support.[67]

Based on the TPR profiles, catalyst reduction temperatures of 350 and 400 °C were selected to obtain partly reduced supports and to study the influence of the degree of support reduction on the product distribution. In the reactor experiments, reduction was performed at 353 °C instead of 350 °C, as the HDO experiments were performed at 350 °C. Using a reduction temperature slightly higher than the reaction temper-

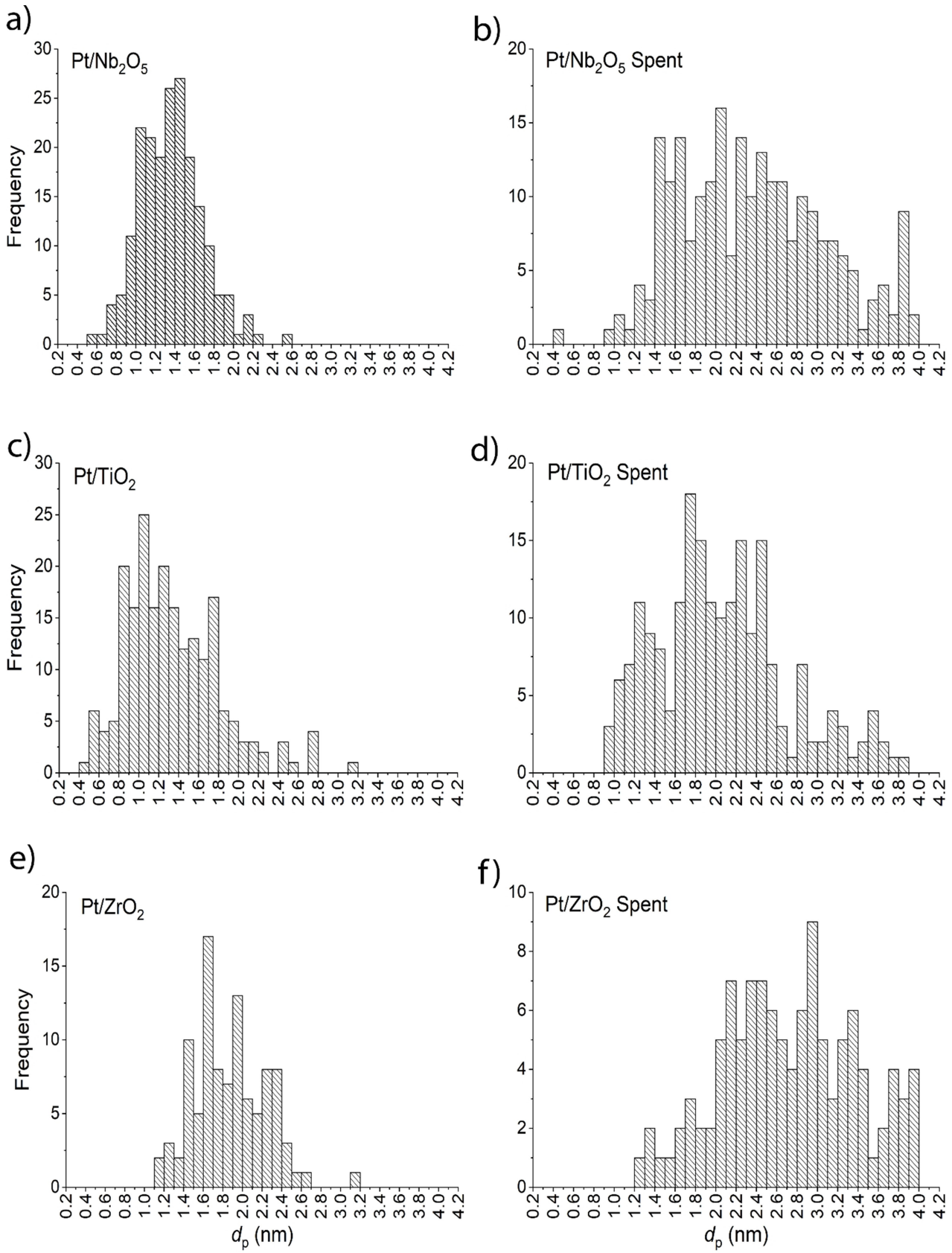

Figure 2. Pt particle size distributions estimated from the STEM images of the fresh and spent catalysts: a) Pt/Nb_2O_5, b) spent Pt/Nb_2O_5, c) Pt/TiO_2, d) spent Pt/TiO_2, e) Pt/ZrO_2 and f) spent Pt/ZrO_2.

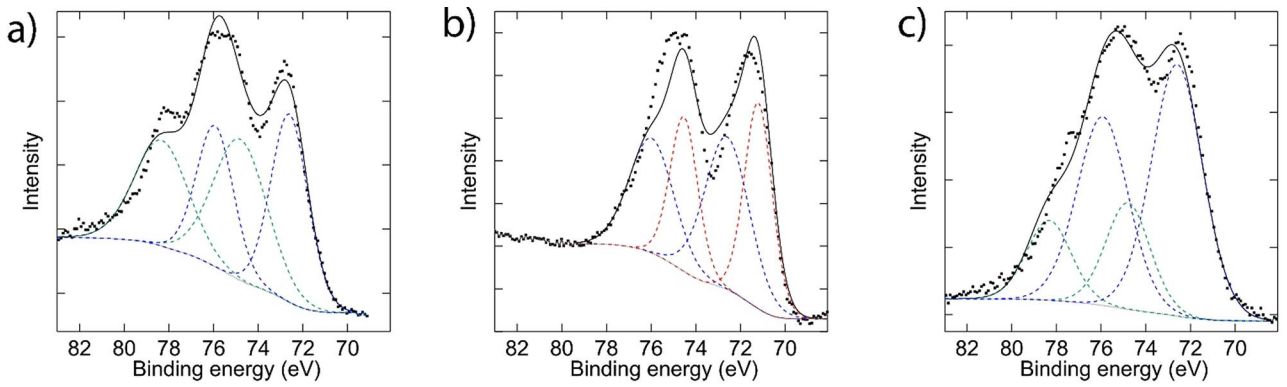

Figure 3. The Pt 4f region in XPS analysis on three different Pt catalysts: a) Pt/Nb_2O_5, b) Pt/TiO_2 and c) Pt/ZrO_2. Three Pt components were used to deconvolute the data, metallic Pt in red, $Pt(OH)_2$ in blue, and PtO_2 in green. All the catalysts were calcined prior to the XPS analysis.

ature was meant to account for possible temperature overshoots during reaction. A temperature difference of 3 °C was the minimum that could be controlled reliably with the given equipment.

Catalytic HDO experiments

The activity and selectivity of Pt catalysts supported on reducible (Nb_2O_5 and TiO_2) oxides and ZrO_2 was investigated at 350 °C with 20 bar H_2 pressure. In previous literature, it has been acknowledged that the reaction temperature affects the thermodynamic equilibrium of hydrotreatment of phenolic model compounds; temperatures above 250 °C promote the formation of aromatic products.[15,37] In this study, preliminary experiments indicated that propylbenzene was not favored even at 300 °C, hence the need for an even higher temperature. The thermodynamic limitations of the system studied in this work are discussed elsewhere.[68]

Batch residence time series and activity of catalysts

For each of the studied catalysts, a set of experiments with different batch residence times was performed in order to generate a batch residence time series. The batch residence time series, see Figure 5, included repeated experiments that presented variations in their results of circa 10 percentage points at most. The differences in the catalysts' activities were apparent at low batch residence times (0.25 $g_{cat}\,min\,g_{reactant}^{-1}$) and were observed in the conversions obtained with each catalyst: 15% with Pt/ZrO_2, 36% with Pt/TiO_2, and 44% with Pt/Nb_2O_5. Full conversion was attained at batch residence times of 4–5 $g_{cat}\,min\,g_{reactant}^{-1}$ with all the catalysts. On the other hand, the initial turnover frequencies (TOFs) were estimated as 1.4 s^{-1} for Pt/ZrO_2, 2.1 s^{-1} for Pt/TiO_2, and 4.1 s^{-1} for Pt/Nb_2O_5. Hence, the most active catalyst (initially), both overall and per active site, was Pt/Nb_2O_5, whereas the least active catalyst was Pt/ZrO_2. No correlation between catalyst acidity and activity in reaction was observed, which is consistent with the literature.[14,33,36,50]

The two main products were propylbenzene and propylcyclohexane. At τ_B of 4–5 $g_{cat}\,min\,g_{reactant}^{-1}$, the selectivities reached a maximum of 60–70% to propylbenzene and 20–30% to propylcyclohexane. The Nb_2O_5 supported catalyst led to a slightly higher selectivity to the aromatic product compared to the other two catalysts. Also, with Pt/Nb_2O_5, the selectivities to the two main products were roughly stable throughout the batch residence time series. Nevertheless, after τ_B of 5 $g_{cat}\,min\,g_{reactant}^{-1}$, the selectivity to propylbenzene decreased and the selectivity to propylcyclohexane increased. By contrast, with the other two catalysts, the selectivities to propylbenzene and propylcyclohexane increased sharply at low batch residence times. The highest obtained propylbenzene selectivity was 77% with a batch residence time of 3.6 $g_{cat}\,min\,g_{reactant}^{-1}$ and a conversion of 98% (Pt/Nb_2O_5).

Experiments with pure supports

The pure supports were tested in 4-propylphenol HDO with batch residence times of approximately 3.7 to 4.0 $g_{cat}\,min\,g_{reactant}^{-1}$. The highest conversion was obtained with Nb_2O_5 (43%), and the conversions for TiO_2 and ZrO_2 were 25% and 12%, respectively. By comparison, similar batch residence times with the three corresponding Pt catalysts resulted in almost 100% conversion. Aside of the lower activity, the pure supports favored different main products from the ones obtained with the Pt catalysts. With TiO_2 and ZrO_2, no propylbenzene or propylcyclohexane were produced. With Nb_2O_5, the propylbenzene selectivity was 0.4% and the propylcyclohexane selectivity was 0.5%. The main product was identified with GCMS-EI and GCMS-CI as 1-methoxy-4-(1-methylpropyl)-benzene (Figure S13 in the Supplementary Material), referred to henceforth as 'aromatic oxygenate' due to the uncertainty in its identification. The aromatic oxygenate was produced with selectivities of 33.6% with Nb_2O_5, 39.3% with TiO_2, and 11.5% with ZrO_2. Additionally, Nb_2O_5 and TiO_2 produced 4-propylcyclohexanol ($\leq$15% selectivity). Nb_2O_5 and ZrO_2 provided toluene with ~3% selectivity. Finally, Nb_2O_5

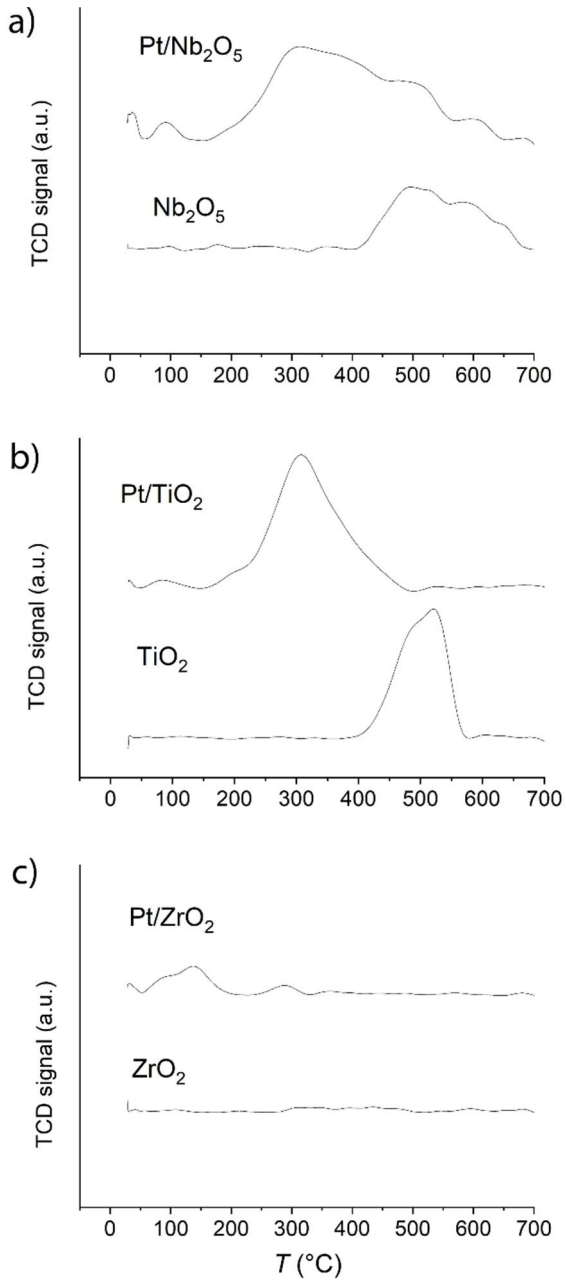

Figure 4. TPR profiles of the Pt catalysts and the supports: a) Pt/Nb_2O_5 and Nb_2O_5, b) Pt/TiO_2 and TiO_2, c) Pt/ZrO_2 and ZrO_2.

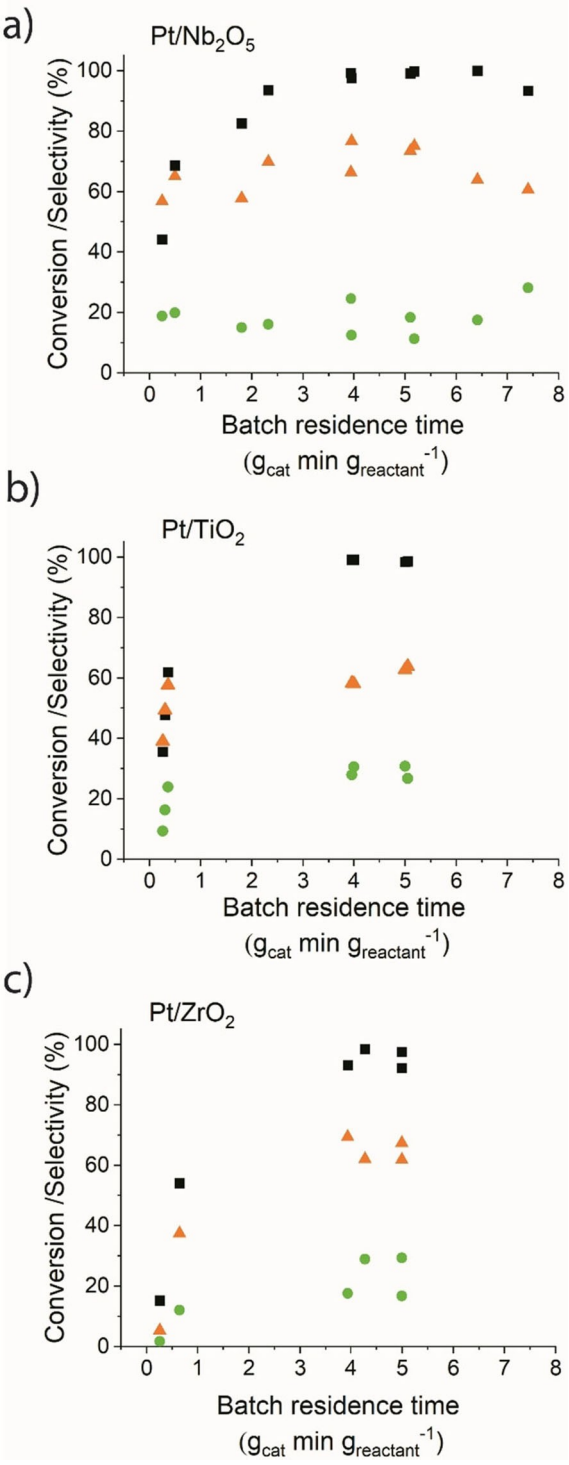

Figure 5. Conversion of 4-propylphenol (■) and the mol-based selectivities to propylbenzene (▲) and propylcyclohexane (●) on a) Pt/Nb_2O_5, b) Pt/TiO_2 and c) Pt/ZrO_2 catalysts as a function of batch residence time. Reaction conditions: ~3% metal loading, 580 mg 4-propylphenol in 27 mL tetradecane, 350 °C, 20 bar H_2.

provided phenol with 3.4% selectivity. Therefore, propylbenzene could not be obtained with the supports without Pt.

Comparison with previous literature

In the literature, the highest aromatic selectivity obtained with HDO of phenols was reported by Zhang et al.[18] They used a bulk MoO_3 catalyst and obtained a benzene selectivity of 99.5% with a phenol conversion of 98% at 340 °C and 6 h in a batch reactor (liquid-phase, *n*-octane solvent, 5 bar H_2 + 30 bar N_2). The mixed gas atmosphere was beneficial, as it prevented the full reduction of the MoO_3 catalyst. Compared to our work, a similar observation about the reaction time was made by Zhang et al.,[18] as after 10 h, the selectivity to benzene had dropped to ~75%, while the selectivity to cyclohexane was ~20%. Whiffen

and Smith[20] also studied an unsupported MoO_3 catalyst in a batch reactor, obtaining 60% selectivity to toluene and 20% to methylcyclohexane, with 80% conversion of 4-methylphenol at 325 °C and 41.4 bar H_2 in decalin solvent (liquid-phase), for 5 h. They also observed a decrease in selectivity to the aromatic product with reaction time, in this case at the expense of isomerization products. Finally, Griffin et al.[15] obtained ~80% selectivity to toluene with 35% 3-methylphenol conversion in a packed-bed reactor operated in vapor-phase at 350 °C and 5 bar H_2 pressure using a Pt/TiO_2 catalyst. The byproducts were ~10% methylcyclohexane, ~8% methylcyclohexanone, and ~2% methylcyclohexanol.

Our best result, 77% aromatic product selectivity at 98% conversion with Pt/Nb_2O_5 catalyst, is among the best results reported in liquid-phase. As had been observed by Zhang et al.[18] and Whiffen and Smith,[20] as well as in the present study, the aromatic selectivity decreased after some time (Figure 5. a). The aromatic products, after being formed, were hydrogenated to cyclohexanes only to some extent.[68] Typical hydrogenation metals present an optimal temperature for aromatic hydrogenation.[69] For example, ~200 °C has been reported for Pt.[69] Aromatic hydrogenation becomes less favored at higher temperatures than the optimum due to a decrease in the adsorbed amounts of the two reactants on the Pt surface.[69]

When comparing our study to other studies with 4-propylphenol as a feed, similar propylbenzene selectivity has been obtained by Ohta et al.[21] and Feng et al.,[19] but using aqueous conditions. Ohta et al.[21] obtained 65% selectivity to 4-propylbenzene with 62% 4-propylphenol conversion at 300 °C (1 h, 20 bar H_2) using Pt/ZrO_2 catalyst. With a bimetallic Pt–Re/ZrO_2 catalyst, the same authors reached 85% selectivity with 67% conversion level in the same conditions.[21] As a comparison, Feng et al.[19] obtained only 54% propylbenzene yield with Re–Ni/ZrO_2 catalyst at 300 °C and 40 bar H_2. However, both studies were conducted in aqueous medium, rather than in an organic solvent. Other works using 4-propylphenol as a feed have focused on cyclohexane production in aqueous medium,[26,70] in a two phase water/dodecane medium,[71] in ester solvents,[72] in octane medium,[73] and solvent-free.[72,73] Although, to our knowledge, only one work on 4-propylphenol HDO to propylbenzene in organic medium have been reported,[45] the hydrotreatment of other phenolic compounds to obtain aromatics as the main product has been attempted in organic solvents.[18,20,39] Also, vapor-phase reaction to obtain aromatic products have been studied.[14,15,33–36]

Selectivity of catalysts with comparable intermediate conversion

Figure 6 presents a comparison of product selectivities with the three catalysts at comparable intermediate conversion levels (44%–54%). Relatively low batch residence times (< 1 $g_{cat}\,min\,g_{reactant}^{-1}$) were chosen in order to compare the activity of the catalysts in conditions where equilibrium was not limiting the reaction. In all cases, propylbenzene was the main product

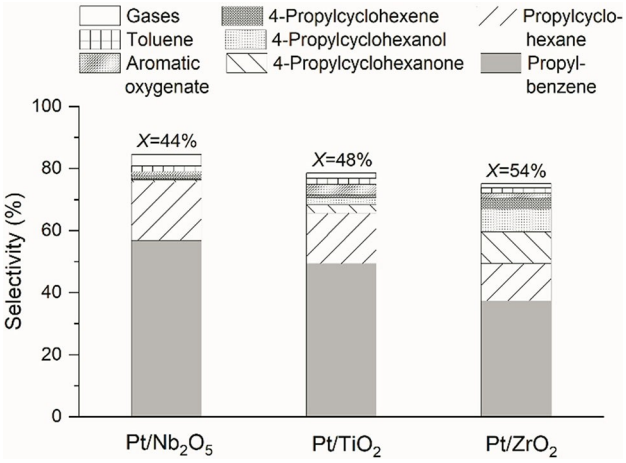

Figure 6. Comparison of product mol-based selectivities on Pt/Nb_2O_5, Pt/TiO_2 and Pt/ZrO_2 catalysts with comparable conversions (44–54%) that were obtained with batch residence times of 0.25, 0.31 and 0.64 $g_{cat}\,min\,g_{reactant}^{-1}$, respectively. Reaction conditions: ~3% metal loading, 580 mg 4-propylphenol in 27 mL tetradecane, 350 °C, 20 bar H_2.

and the highest selectivity towards it was obtained with Pt/Nb_2O_5 catalyst. Pt/TiO_2 provided an only slightly lower selectivity to propylbenzene, but with Pt/ZrO_2, a significantly lower selectivity was obtained. Moreover, a clear difference was observed with the selectivity to other products, as Pt/ZrO_2 provided a significantly higher selectivity to 4-propylcyclohexanone, 4-propylcyclohexanol and 4-propylcyclohexene than the other catalysts. Thus, the Pt/ZrO_2 catalyst was less active for full deoxygenation than the catalysts with reducible supports. A similar observation was made by Griffin et al.,[15] who studied 2-methylphenol deoxygenation in vapor-phase with reducible and irreducible supports, namely Pt/TiO_2 and Pt/C, and concluded that reducible metal oxide supports played a key role in promoting deoxygenation.[15]

In addition to liquid products, all the catalyst produced gas products that were also analyzed. With comparable conversion levels, the mole-based selectivities to methane and ethane were, respectively, 0.35% and 2.0% with Pt/Nb_2O_5, 0.53% and 1.0% with Pt/TiO_2, and 0.80% and 0.43% with Pt/ZrO_2. The produced moles of ethane roughly matched the produced moles of toluene with Pt/ZrO_2 (0.04 mmol). However, with Pt/Nb_2O_5, the produced ethane (0.18 mmol) substantially exceeded the toluene (0.03 mmol), and with Pt/TiO_2, the produced ethane (0.09 mmol) was more than the double of the toluene (0.04 mmol). The matching selectivities of toluene and ethane with Pt/ZrO_2 appear to indicate that the propyl sidechain was cracked. On the other hand, with Pt/Nb_2O_5 and Pt/TiO_2, none of the detected products other than toluene appear to evidence sidechain cracking to ethane. Thus, given the excess of ethane compared to toluene produced on Pt/Nb_2O_5 and Pt/TiO_2, a more complex decomposition of C_9 molecules likely occurred on these catalysts.

The overall mass-based yields of gaseous products, including hydrocarbons, CO, and CO_2, with the catalyzed experiments increased from ~0.001% at 44–54% conversion to ~0.02% at

full conversion. Likewise, the overall gas yield with the catalyst-free blank was ~0.02%. The catalyzed experiments provided mostly methane and ethane, whereas the non-catalyzed experiment provided mostly CO. In the catalyzed experiments, CH_4 might have been formed by CO hydrogenation over the catalyst.

Catalyst reduction temperature

The effect of reduction temperature on catalytic activity and selectivity was studied with the Nb_2O_5 and TiO_2 supported catalysts. In order to investigate how the extent of support reduction affected product distribution and catalyst activity, two reduction temperatures (353 °C and 400 °C), higher than the HDO reaction temperature (350 °C), were chosen based on the TPR study (Figure 4a and b). The results are presented in Figure 7 for Pt/Nb_2O_5 catalyst and in Figure 8 for Pt/TiO_2 catalyst.

At high batch residence times (~4.0 $g_{cat}\,min\,g_{reactant}^{-1}$), conversions close to 100% were obtained with both catalysts. The Pt/Nb_2O_5 catalyst reduced at 400 °C provided more hydrogenated product, propylcyclohexane, than the aromatic product, whereas the catalyst reduced at 353 °C provided the same products in reverse order of abundance (Figure 7). This result stands out among the experiments reported in this work, in which propylbenzene was the most abundant product. At low batch residence times (~0.26 $g_{cat}\,min\,g_{reactant}^{-1}$), no significant differences in product distribution were observed with Pt/Nb_2O_5 catalyst, although the obtained conversion was slightly lower for high reduction temperature. On the contrary, the Pt/TiO_2 catalyst resulted in slightly less propylbenzene and slightly more cyclohexane after reduction at 400 °C compared to the reduction at 353 °C (Figure 8); however, the differences in selectivity were less than the experimental uncertainty. At low batch residence time, the Pt/TiO_2 catalyst had roughly 10% selectivity to the aromatic oxygenate regardless of the reduction temperature.

Barrios et al. studied the effect of reduction temperature (300 or 500 °C) on the reaction rate of phenol HDO with Pd/Nb_2O_5.[14] The reaction rate dropped significantly with the higher reduction temperature, due to the almost full coverage of the Pd particles by NbO_x species formed at high temperature.[14] Kon et al.[51] also studied the effect of reduction temperature (100 to 300 °C) on Pt/Nb_2O_5's activity in fatty acids HDO. The activity was higher with the catalyst reduced at 300 °C. They attributed the higher activity to the partial coverage of NbO_x on the Pt particles, which was also referred as partial SMSI state of the catalyst.[51] Based on our TPR of the Pt/Nb_2O_5 catalyst (Figure 4a), which had a similar thermal history as Kon et al.'s[51] catalyst, the reduction of the support started approximately at 200 °C, which likely explains why Kon et al.[51] observed an increase in activity by increasing the reduction temperature from 100 °C to 300 °C. Hence, to obtain partial coverage of the metal, reduction temperatures $\leq$200 °C and $\geq$350 °C seem less beneficial for Pt or Pd catalysts supported on Nb_2O_5.

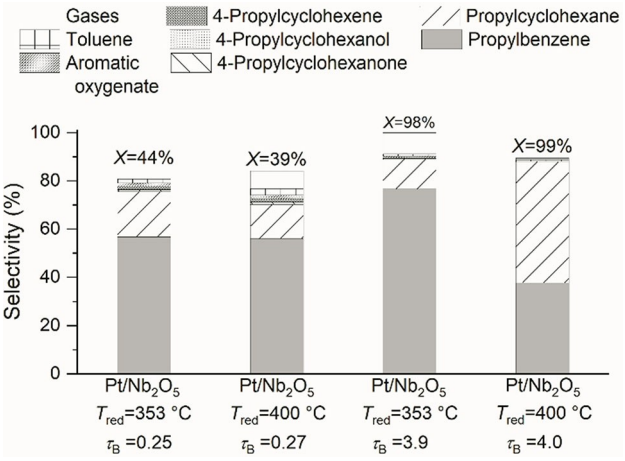

Figure 7. The effect of catalyst reduction temperature (353 or 400 °C) on the product mol-based selectivities obtained with Pt/Nb_2O_5 catalyst with different batch residence times (τ_B ~0.26 or 4.0). The unit of τ_B is $g_{cat}\,min\,g_{reactant}^{-1}$. Reaction conditions: ~3% metal loading, 580 mg 4-propylphenol in 27 mL tetradecane, 350 °C, 20 bar H_2.

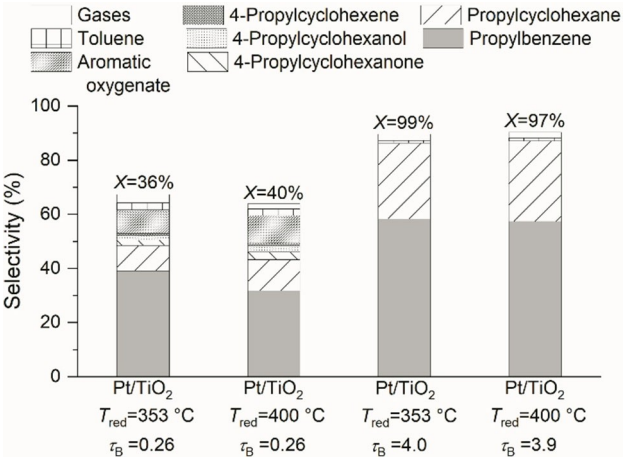

Figure 8. The effect of catalyst reduction temperature (353 or 400 °C) on the product mol-based selectivities obtained with Pt/TiO_2 catalyst with different batch residence times (τ_B ~0.26 or 4.0). The unit of τ is $g_{cat}\,min\,g_{reactant}^{-1}$. Reaction conditions: ~3% metal loading, 580 mg 4-propylphenol in 27 mL tetradecane, 350 °C, 20 bar H_2.

With Pt/TiO_2, the lower reduction temperature (<353 °C) might have created a favorable coverage of Pt by TiO_x to optimize the propylbenzene selectivity. This is supported by TPR (Figure 4b), which shows the maximum of the support's reduction peak already at around 300 °C.

Characterization and reusability of spent catalysts

Spent catalysts were characterized and used a second time in HDO to study their deactivation. Based on the physicochemical characterization, deactivation was observed with all the catalysts, but some differences were also observed.

It can be observed form Figure S1 that the physisorption isotherms and pore size distributions had the least changes with Pt/ZrO_2 catalyst. In the case of the TiO_2 supported catalyst, most of the mesopores between 4 to 10 nm disappeared and the surface area of the Pt/TiO_2 catalyst decreased to half. The metal dispersion and the calculated average particle diameters (from chemisorption and TEM) for the spent catalysts are listed in Table 1, and the chemisorption isotherms of spent catalysts are presented in Figure S2. In the dispersion and particle size calculations, the metal loading for the spent catalysts was 2% estimated by XRF. As the metal contents of all the spent catalysts were similar, it did not account for the differences observed in chemisorption. The Pt dispersion on Nb_2O_5 decreased by ~70% and on ZrO_2, by ~60%. The Pt dispersion on TiO_2 decreased less, about by 30%. Compared to the particle sizes estimated from the STEM images (Figure 1, Table 1), the particle sizes calculated by chemisorption seemed to be too high for the spent Pt/Nb_2O_5 and Pt/ZrO_2 catalysts. The difference could be caused by the deactivation of the metal sites causing them to be unavailable for chemisorption. This does not necessarily mean that the particles have agglomerated, as they could be partly covered with solid deposits, the support (due to SMSI, especially on Nb_2O_5), or impurities. Thus, the particle sizes estimated from the STEM images might be more reliable. In the X-ray diffraction (XRD) analysis, no Pt peaks were visible in the spent catalysts. The highest increase in particle size was observed with the Nb_2O_5 support, which also experienced the most severe loss in metal dispersion.

TGA thermograms (Figure S9 in the Supplementary Material) were recorded for the spent, unwashed catalysts in order to estimate the amount of combustible material deposited on the catalysts. First, the samples were dried in nitrogen flow up to 260 °C (boiling point of tetradecane 254 °C) after which the combustion was performed in oxygen flow up to 900 °C. The catalysts were exposed to the ambient atmosphere between the steps, thus the mass loss below 100 °C in the combustion ramp is mainly due to moisture. In the case of Pt/Nb_2O_5 and Pt/ZrO_2 catalysts, $\leq$2% of the mass was combustible after drying. For the Pt/TiO_2 catalyst, almost 3% of the mass was combustible, indicating more carbonaceous deposits on TiO_2 supported catalyst. These amounts of carbonaceous deposits correspond to 0.05% to 0.35% mass-yield with respect to the initial reactant, although coke formation from the solvent cannot be discarded. The higher amount of carbonaceous deposits found in the TiO_2 catalyst compared to the other two could explain the severe loss of pores by filling of the pores to some extent, although the collapse of the pore structure could also have led to the decrease of the surface area. After the experiments with Pt/TiO_2 catalyst, some fine catalyst powder was recovered from the reactor, indicating that attrition of the particles had occurred.

The spent catalysts we tested again in the reaction (Figure 9). Because of different fresh catalyst activities (Figure 5), also different residence times were selected for the tested catalysts. The 4-propylphenol conversion dropped by 50% with Pt/Nb_2O_5, 44% with Pt/TiO_2, and 46% with Pt/ZrO_2 compared to fresh catalysts with the same batch residence times. This loss of

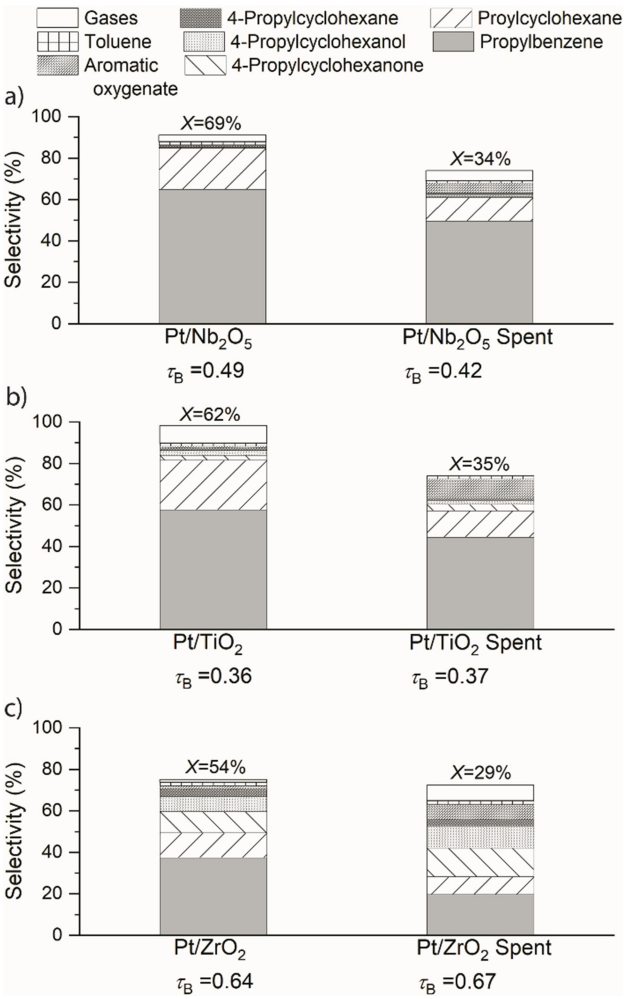

Figure 9. Conversion (X) of 4-propylphenol and product mol-based selectivities obtained with fresh and spent catalysts : a) fresh and spent Pt/Nb_2O_5, b) fresh and spent Pt/TiO_2, c) fresh and spent Pt/ZrO_2. The unit of τ_B is $g_{cat}\,min\,g_{reactant}^{-1}$. Reaction conditions: ~3% metal loading, 580 mg 4-propylphenol in 27 mL tetradecane, 350 °C, 20 bar H_2. Gas analysis was not available for spent Pt/TiO_2.

activity can be partly explained by the lower metal loading of the spent catalysts compared to the fresh ones (Table 1). In all cases, also the propylbenzene and propylcyclohexane selectivities decreased. With all the spent catalysts, the selectivity towards the aromatic oxygenate increased compared to the fresh catalysts. With Pt/ZrO_2, the selectivity of other side products, such as 4-propylcyclohexanone and 4-propylcyclohexanol, also increased.

Other researchers have also reported deactivation studies in water phase[21] and in vapor-phase.[36] De Souza et al.[36] investigated deactivation of Pd catalyst supported on various supports including ZrO_2 and TiO_2. In continuous gas phase reaction of phenol, significant deactivation was observed with all the tested supports after 20 h of reaction, excluding those containing CeO_2.[36] In addition to the observed lower conversion, also the product distribution changed towards side products instead of deoxygenated products[36] as took place with our spent Pt/ZrO_2 catalyst also. The change in product

distribution was explained with the loss of Pd and support interaction due to carbon deposition; metal sintering; and loss of Lewis acid sites on the support.[36] Teles et al.[22] also reported deactivation of various metals (Pt, Pd, Rh, Ru, Cu, Ni and Co) on ZrO_2. The main reasons for deactivation were metal sintering and the decrease of the number of oxophilic sites caused by strong adsorption of reaction intermediates.

Conclusions

The HDO of 4-propylphenol to propylbenzene, as a model for upgrading biocrudes, was studied in a batch reactor (liquid organic phase) with target 3 wt.% Pt catalysts supported on Nb_2O_5, TiO_2 and ZrO_2. The main product with all the catalysts was propylbenzene at 350 °C and 20 bar H_2 pressure, whereas propylcyclohexane was the main side product. The Pt/Nb_2O_5 catalyst had the highest selectivity to the aromatic product, 77% at 98% conversion, which is among the best results reported in the literature. The TiO_2 and ZrO_2 supported catalysts reached maximum propylbenzene selectivities of 64% and 69%, respectively.

The most active catalyst was Pt/Nb_2O_5, which had the initial TOF of 4.1 s^{-1} compared to the initial TOFs of 1.4 s^{-1} for Pt/ZrO_2 and 2.1 s^{-1} for Pt/TiO_2. The activity enhancement of Nb_2O_5 and TiO_2 compared to ZrO_2 was discussed to be due to oxophilic NbO_x and TiO_x species created during catalyst reduction in the vicinity of hydrogenating Pt sites. The reusability of the catalysts was investigated by testing the spent catalysts in the reaction. For all the spent catalysts, the conversions dropped by approximately 50% compared to the fresh catalysts with the same batch residence time. The selectivity of the spent Pt/ZrO_2 catalyst changed towards oxygenated side products (4-propylcyclohexanone and 4-propylcyclohexanol), whereas with the other spent catalysts, mainly propylbenzene and propylcyclohexane were produced.

In this study, high catalyst activity and selectivity to propylbenzene were obtained in 4-propylphenol HDO over Pt catalysts with reducible supports. These results further highlight the opportunity to use biocrudes as a source of aromatic fuel components and chemicals.

Experimental Section

Materials

The chemicals used in experiments and GC calibrations included 4-propylphenol (≥97%), tetradecane (≥99%), propylbenzene (98%), propylcyclohexane (99%), 4-propylcyclohexanone (≥99.0%) and 2-isopropylphenol (98%) from Sigma-Aldrich. 4-Propylcyclohexanol (>98.0%, cis- and trans- mixture) was obtained from Tokyo Chemical Industry. Karl-Fisher titration chemicals included Merck's Apura® two component titrant containing MeOH and iodine, Merck's Apura® solvent for volumetric Karl-Fisher titration containing MeOH and imidazole, and Merck's Apura® water standard (1% H_2O). All the chemicals were used without further purification.

The gases used in experiments and catalyst characterization were purchased from Oy AGA Ab: H_2 (purity 5.0), He (purity 5.5), N_2 (purity 5.0), CO (Linde, purity 4.7), a mixture of 2% H_2 (purity 5.0) in Ar (purity 5.0), a mixture of 5% NH_3 (purity 5.0) in He (purity 5.0) and a mixture of 5% CO_2 (purity 5.0) in He (purity 5.0). The gases used in analytics were H_2 (purity 5.0), He (purity 4.6), Ar (purity 5.0), synthetic air (purity 5.0), and N_2 (purity 5.0). Two calibration gas mixtures were utilized, the first contained 40 mol% N_2, 5 mol% CH_4, 10 mol% C_2H_6, 5 mol% C_2H_4, 10 mol% C_3H_8, 5 mol% C_3H_6, 5 mol% C_2H_2, 10 mol% C_4H_{10} and 10 mol% isobutane. The second calibration gas mixture contained 15 vol.% CO, 15 vol.% CO_2, 15 vol.% H_2, 40 vol.% N_2 and 15 vol.% CH_4. The calibration gas mixtures were also obtained from Oy AGA Ab.

Catalytic materials included catalyst supports: niobium oxide hydrate ($Nb_2O_5 \times nH_2O$, HY-340) from Companhia Brasileira de Metalurgia e Mineração, anatase TiO_2 from Alfa Aesar and monoclinic ZrO_2 from Saint-Gobain NorPro. Metal precursor was Pt (IV)nitrate solution (15% w/w Pt) from Alfa Aesar.

Catalyst Preparation

Niobium oxide hydrate powder was thermally treated at 270 °C in synthetic air (7 h, heating rate 100 °C h^{-1}), pressed into tablets, ground and sieved to 0.25–0.42 mm particles. The other supports were also ground and sieved to the size range of 0.25–0.42 mm. All the supports were calcined in synthetic air: ZrO_2 at 600 °C for 10 h (heating rate 100 °C h^{-1}), TiO_2 at 500 °C for 7 h (heating rate 100 °C h^{-1}), and Nb_2O_5 particles, a second time, at 500 °C for 7 h (heating rate 100 °C h^{-1}). The Nb_2O_5 was calcined in two steps, 270 °C and 500 °C, to make the prepared tablets stronger. The active metal containing catalysts (nominal 3 wt.%) were prepared by incipient wetness impregnation. Appropriate amounts of aqueous solutions of metal precursor were used, and the pore volumes of the supports were estimated by the water uptake capacity (ca. 40% of support's mass for all the calcined supports). The prepared catalysts were dried at room temperature (RT) for 5 h and in an oven at 100 °C overnight. Finally, the catalysts were thermally treated in synthetic air at 350 °C for 3 h with a heating ramp of 30 °C h^{-1}. The catalyst after this treatment is referred to as 'fresh catalyst' throughout this work.

Appropriate amount of catalysts (to match the desired batch residence time, see Section Calculations.) were reduced at 20 bar H_2 for 1 h in the same batch reactor as used in the HDO experiments, a 100 mL Parr with 200 rpm mixing. The reduction temperature was either 353 or 400 °C.

Catalyst Characterization

Fresh catalysts were characterized after preparation and thermal treatments. For TPD and chemisorption measurements, the catalysts were also reduced prior to the analysis as described later in this Section. Spent catalysts were separated from the reaction mixture, and catalysts from selected experiments (τ_B approximately 4 and 5 $g_{cat}\,min\,g_{reactant}^{-1}$, see Figure 5) were mixed together to obtain enough spent catalysts for characterization. The mixed spent catalysts were washed with EtOH to remove the remained liquid from the reactor using a vacuum filtration system. After washing, the catalysts were dried in a 100 °C oven overnight. For TGA, unwashed spent catalyst was used.

XRF was measured with a PANalytical Axios Max wavelength dispersive spectrometer with an X-ray source of SST-max. The samples were placed into a sample cup on a Mylar film without any pretreatment. The analysis was used to obtain an estimation of the Pt loading in the fresh and spent catalysts.

Nitrogen physisorption isotherms (liquid N_2, −196 °C) were recorded with a Thermo Scientific Surfer equipment. The catalyst samples were weighted to quartz glass burettes (ca. 200 mg), and the fresh catalysts were evacuated at 300 °C for 3 h and the spent catalysts at 120 °C for 5 h prior to the measurements. Specific surface areas were calculated from the isotherms according to the BET method.[74] The cumulative pore volumes and the pore size distributions were calculated based on the Barrett-Joyner-Halenda (BJH) method.[75]

Carbon monoxide chemisorption isotherms at 25 °C were measured with the Thermo Scientific Surfer equipment. Prior to the measurements, the catalyst samples (fresh and spent) were weighted to U-shaped quartz burettes (ca. 150–200 mg) and supported with quartz glass wool. The samples were reduced in hydrogen flow at 290 °C for 3 h and degassed at the same temperature down to 10^{-5} Torr for 2 h. At first, the total adsorption isotherm was recorded, which was followed by degassing down to 10^{-5} Torr. After the reversibly adsorbed gas was removed, the second isotherm containing only the reversible adsorption was recorded. After measurements, the samples were weighted once more to obtain the dry weight of the sample, which was used in calculations. The irreversible monolayer volume was obtained from the linear regression of the subtracted irreversible isotherm to zero pressure. Finally, metal dispersion and particle size were calculated as described elsewhere:[60] the adsorption stoichiometry for CO was assumed 1 and the metal particles were assumed to be spherical.

STEM images were taken from the fresh and spent catalysts using a JEOL JEM-2200FS Double Cs-corrected transmission microscope with 200 kV acceleration voltage. Energy-dispersive X-ray spectroscopy (EDS) was applied to detect the chemical elements present in the sample. Samples for STEM analyses were drop-casted from ethanol dispersions onto copper grids coated with ultrathin carbon film (< 10 nm thickness). To estimate the average size of the metal nanoparticles deposited on the support, several particles were measured manually from the images using Gatan DigitalMicrograph-software: 196 for fresh Pt/Nb_2O_5, 183 for fresh Pt/TiO_2 and 100 for fresh Pt/ZrO_2. In the case of the spent catalysts, 188 particles were measured for Pt/Nb_2O_5, 208 for Pt/TiO_2 and 124 for Pt/ZrO_2.

XRD was used to detect the crystallographic phases in the catalysts. The equipment was a PANalytical X'Pert PRO MPD Alpha-1 diffractometer with Cu Kα1 radiation (45 kV and 40 mA). The X-ray scanning range was 4.5° to 120° (2θ) with a step of 0.0263°. Prior to the analysis, the samples were ground.

The X-ray photoelectron spectroscopy (XPS) measurements were made for the fresh catalysts using Kratos Axis Ultra system, equipped with a monochromatic AlKα X-ray source. All measurements were performed with 0.3 mm × 0.7 mm analysis area and the charge neutraliser on. The wide scans were performed with 80 eV pass energy and 1 eV energy step and the high resolution scans were performed with 20 eV pass energy with 0.1 eV steps size. The energy calibration was made using the adventitious carbon C1s component at 284.8 eV. All decompositions were made with CasaXPS using GL(30) peaks (product of 30% Lorenztian and 70% Gaussian).

The acidity and basicity of the fresh catalysts were analyzed with TPD of ammonia (NH_3—TPD) and carbon dioxide (CO_2—TPD) by an AutoChem II 2920 device. Prior to the NH_3-TPD analysis, the sample (about 45 mg) was reduced with H_2 from RT to 353 °C (5 °C min^{-1}) and kept at 353 °C for 60 min. Then, the sample was cooled down to 100 °C followed by adsorption of 5% NH_3 in He (at 100 °C) for 60 min and flushing with He for 30 min in order to remove the weakly bonded NH_3. The NH_3 desorption was carried out from 100 to 600 °C (10 °C min^{-1}), then left for 10 min at 600 °C. For the CO_2—TPD (same samples after NH_3-TPD), similar reduction treatment was done as for the NH_3-TPD. After the reduction, the catalysts were cooled down to 50 °C and flushed with He for 5 min. The adsorption of 5% CO_2 in He was performed at 50 °C for 60 min after which the weakly bonded CO_2 was flushed by He flow for 30 min (50 °C). The desorption of CO_2 was conducted by He from 50 to 600 °C, then kept at 600 °C for 10 min. The concentrations of desorbed NH_3 and CO_2 were analyzed by a thermal conductivity detector (TCD). The gas flow rate was 50 mL min^{-1} during the whole TPD analysis. The total acidity (from NH_3—TPD) was determined by integration of the area between 100–600 °C and the total basicity (from CO_2—TPD) was determined by integration of the area between 50–600 °C. The conversion to desorbed gas volume was performed using the software of the AutoChem device after calibration with a series of gas concentrations. For integration, the baseline was corrected, assuming a linear baseline between the beginning and the end of each peak.

TPR was conducted with an Altamira AMI-200 equipment having a TCD. The fresh samples (50 mg) were weighed in a U-shaped flow through quartz tube and were supported with quartz wool. Prior to TPR measurements, the samples were dried in He flow of 40 mL min^{-1} at 350 °C for 1 h. After drying, the samples were cooled to 30 °C and a heating ramp of 5 °C min^{-1} to 700 °C was performed in 2% H_2/Ar flow (40 mL min^{-1}). A cold trap filled with CO_2 ice was used between the sample tube and the TCD to prevent moisture from entering the detector.

TGA was used to determine the amount of carbonaceous solids deposited on the spent catalysts during the HDO reactions. The equipment was a TA Instruments' TGA Q500. Approximately 10 mg of spent, unwashed catalyst was dried in pure nitrogen from RT up to 260 °C with a heating rate of 10 °C min^{-1}. The drying ramp was followed by a 30 min isothermal hold at 260 °C (the boiling points of tetradecane, propylphenol, propylbenzene, and propylcylclohexane are < 255 °C). Afterwards, the dried sample was heated up from ~75 °C to 900 °C (10 °C min^{-1}) with pure oxygen.

HDO Experiments

The HDO experiments were conducted in a 100 mL Parr batch reactor. The catalyst was dried and reduced in situ. The drying was performed in N_2 atmosphere at 180 °C for 1 hour and the reduction, in 20 bar H_2 at 353 or 400 °C for 1 hour. The reactor was stirred at 200 rpm during reduction. Afterwards, the reactor was cooled to room temperature and kept overnight in H_2 pressure. Before the experiments, the reactor was vented to atmospheric pressure and heated up to the desired reaction temperature (350 °C). Once the temperature was attained, about 580 mg of reactant, dissolved in 27 mL of tetradecane, was injected into the reaction chamber from the feed vessel of the reactor with the aid of hydrogen. The reactor was pressurized up to 20 bar H_2 and a mixing rate or 645 rpm was applied. The reaction was allowed to proceed for a given time to match the desired batch residence time. Afterwards, the reactor was cooled to room temperature. The reaction time was counted from the moment of injection of the reaction mixture to the start of the cooling. When the reactor was at room temperature, the gas phase was sampled, the reactor was vented, and the product and the catalyst were recovered.

To study the reusability of the catalysts, the catalysts recovered after HDO experiments were washed in ethanol over a filtration funnel and dried overnight in an oven at 100 °C. The washed catalysts were dried and reduced in situ before HDO reaction by the same procedure as the fresh catalysts.

In order to ensure that all experiments were performed under stable conditions, all HDO experiments were run for at least 10 min.

This time constraint, along with the small amount of reactant used, favored conversions >80%. In order obtain lower conversions, both the amount of catalyst and the reaction time were adjusted. Hence, the reaction was studied with respect to batch residence time instead of simply reaction time.[76,77] Table S1 in the Supplementary Material lists the reaction times and amounts of catalyst and reactant used in all experiments. Furthermore, the external mass transfer limitations were assessed experimentally and with calculations (Section 5 in the Supplementary Material) and they were determined to be negligible. Internal mass transfer limitations were also negligible, according to the Weisz-Prater criterion (Section 6 in the Supplementary Material).

Product Analysis

Organic products were identified with a gas chromatograph (GC) from Agilent, which was equipped with a Zebron ZB-wax Plus column (60 m×0.25 mm×0.25 μm) and an electron-impact mass spectrometer (GCMS-EI, 7890–5975). The injection of 1 μL sample was conducted at 250 °C with 0.6 mL min^{-1} flow and 80:1 split ratio. The temperature program started with a 2 min hold at 60 °C, followed by heating at 7 °C min^{-1} until 160 °C with a 3 min hold, heating at 5 °C min^{-1} to 200 °C with a 6 min hold, and finally heating at 10 °C min^{-1} to 240 °C with 1 min hold. The electron impact ionization MS detector was operated at 70 eV, with a quadrupole m/z scan range of 30–500 amu. The NIST MS library was used to aid spectral interpretation. Furthermore, the product and solvent peaks were deconvoluted with NIST's Automated Mass Spectral Deconvolution and Identification System (AMDIS) in search for possible overlapping products. The identified products are listed in Table S2 of the Supplementary Material. In one case, the identification with GCMS-EI was uncertain; hence a second technique was used, GCMS with chemical ionization (GCMS-CI). For GCMS-CI (Thermo Scientific Trace 1300 ISQ), the same chromatographic column and method were used as for GCMS-EI. The CI parameters were 180 °C, positive polarity, and methane (1.5 mL min^{-1}) reagent gas.

The quantification of the liquid organic products was conducted with a GC from HP (6890 Series) equipped with a flame ionization detector (FID) and using the same column and method as described with the GC-MS. The products were calibrated using 2-isopropylphenol as the internal standard. For the products that were not calibrated (e.g. 4-propylcyclohexene and 1-propylcyclohexene), the response factor was estimated according to the effective carbon number method proposed by Scanlon and Willis.[78] The effective carbon number corrections were taken from Jorgensen et al.[79]

For some organic products, as well as for the solvent, the water content was analyzed using a SI Analytics' volumetric Karl-Fisher titrator (TitroLine 7500 KF) calibrated with a water standard. The water concentrations were 0.007 wt.% for the measured products and also 0.007 wt.% for the fresh solvent. Hence, it is likely that the water formed during HDO did not dissolve into the organic phase. Instead, it is possible that the water formed a second liquid-phase in such a small amount (<76 mg), that it was lost during product recovery.

Gaseous products were analyzed by a GC from Agilent (6890 Series) with a FID and a TCD. The GC was calibrated with an Oy AGA Ab calibration gas mixture, which enabled quantitative analysis. The TC detector was connected to two columns: HP-PLOT/Q (30 m× 0.53 mm×40 μm) and HP Molesieve (30 m×0.53 mm×25 μm), and was used for the analysis of CO, CO_2, H_2 and N_2. Hydrocarbons were analyzed with the FID connected to a HP-AL/KCL column (50 m× 0.32 m×8 μm). The heating program started from 40 °C (inlet temperature 200 °C) with a 9.5 min hold. The heating rate was 10 °C min^{-1} up to the final temperature of 200 °C.

Calculations

Conversion (X) is defined as [Eq. (1)]:

$$X = \frac{n_{A,0} - n_{A,f}}{n_{A,0}} \tag{1}$$

where $n_{A,0}$ is the molar amount of reactant at the beginning of the experiment and $n_{A,f}$ is the molar amount of reactant at the end. Mol-based selectivity (S_n) is defined as [Eq. (2)]:

$$S_n = \frac{|\nu_A| n_P}{\nu_P \left(n_{A,0} - n_{A,f}\right)} \tag{2}$$

where n_P is the molar amount of product obtained in the experiment, ν_A is the stoichiometric factor of 4-propylphenol, and ν_P is the stoichiometric factor of the product. Because the reaction routes to many products are unknown, $\nu_A = -1$ was taken as a reference. The stoichiometric factors of the products were calculated as [Eq. (3)]:

$$\nu_P = \frac{N_{C,A}}{N_{C,P}} \tag{3}$$

where $N_{C,A}$ is the number of C atoms in propylphenol and $N_{C,P}$ is the number of C atoms in the product. Equation 3 did not apply in the cases of benzene, toluene, ethylbenzene, cyclohexane, methylcyclohexane, phenol, and 2-ethylphenol, for which it was assumed that $\nu_P = 1$. Mol-based yield (Y_n) is defined as [Eq. (4)]:

$$Y_n = \frac{|\nu_A| n_P}{\nu_P n_{A,0}} \tag{4}$$

Mass-based selectivity (S_m) and yield (Y_m) were calculated analogously to equations (2) and (4), except that stoichiometric factors were not included.

The GC analysis of the gas phase returned the molar fractions of the components in a sample of the gas phase. In order to determine the molar amounts of the gases, and hence their masses, the total gas moles were calculated with the ideal gas law from the temperature and absolute pressure in the reactor at the time of the sampling. The volume occupied by the gas was calculated taking into account the volume occupied by the liquid-phase, which in turn was calculated from the density of tetradecane at the given conditions (see Section 4 in the Supplementary Material).

In order to overcome constraints in reaction times and to minimize the influence of variations in the weighed amounts of reactant and catalyst, the HDO reactions were studied with respect to batch residence time (τ_B, $g_{cat}\,min\,g_{reactant}^{-1}$) [Eq. (5)]:[76,77]

$$\tau_B = \frac{m_{cat}}{m_A} t \tag{5}$$

where m_{cat} is the mass of catalyst (g), m_A is the initial mass of reactant (g), and t is the reaction time (min).

Initial turnover frequencies (TOF_0, s^{-1}) of 4-propylphenol on the catalysts were estimated as [Eq. (6)]:

$$TOF_0 = \frac{r_{\varphi,0}}{\Gamma_{cat}} \quad (6)$$

where $r_{\phi,0}$ is the initial reaction rate (mol g_{cat}^{-1} s^{-1}) and Γ_{cat} is the molar amount of surface metal sites per gram of catalyst (mol g_{cat}^{-1}), assumed to be equal to the irreversible chemisorption capacity of the catalyst (Table 1). The initial reaction rate was estimated by fitting a polynomial function (f) to a contact time series ($m_A\tau$, [g_{cat} s]) of reactant molar amount (n_A). Afterwards, f was derived with respect to $m_A\tau$ and evaluated at $m_A\tau = 0$ [Eq. (7)]:

$$r_{\varphi,0} \approx \left[-\frac{d}{d(m_A\tau)}\left(f(m_A\tau, n_A)\right)\right]_{m_A\tau=0} \quad (7)$$

The carbon balances of the conducted experiments are presented in Table S3 along with the corresponding mass balances. The carbon balances describe the moles of carbon present in the quantified products and in the unconverted reactant as a percentage of the carbon moles present in the reactant fed to the reactor [Eq. (8)]:

$$B_C = \frac{N_{C,A}n_{A,f} + \sum_i N_{C,P,i}n_{P,i}}{N_{C,A}n_{A,0}} \quad (8)$$

The solvent and its cracking products (10^{-5} %) were not accounted in the carbon balances. In some cases, the carbon balances were > 100 %, which can be explained by uncertainties in the calculation of the stoichiometric factors (Equation 3). The mass balances express the total quantified mass of gas, liquid, and solid recovered after the experiments as a percentage of the total mass of reactant, solvent, and catalyst added to the reactor. Table S3 includes the sums of mass-based selectivities per experiment (ΣS_m), representing the closure of the mass balances in terms of the products against the reactant (excluding the solvent) [Eq. (9)]:

$$100\,\% = \frac{\sum_i m_{P,i}}{m_{A,0} - m_{A,f}} + \frac{loss}{m_{A,0} - m_{A,f}} = \Sigma S_m + loss\% \quad (9)$$

Acknowledgements

The authors acknowledge Companhia Brasileira de Metalurgia e Mineração (CBMM) for providing the niobium oxide hydrate. The authors thank Dr. Hua Jiang from Aalto University OtaNano – Nanomicroscopy Center (Aalto-NMC) for the acquisition of TEM images. Ilkka Välimaa from Aalto University is thanked for helping with X-ray analysis and Dr. Yingnan Zhao with the Altamira AMI-200 equipment. Dr. Zouhair El Assal is thanked for performing the TPD measurements. Heidi Meriö-Talvio is thanked for the help in the identification of 1-Methoxy-4-(1-methylpropyl)-benzene. The national BioEconomy and Raw Materials Research Infrastructure (RAMI) are acknowledged for equipment support. Neste Corporation funded this work. E. M. acknowledges a grant from Aalto University and J. L. G. E. acknowledges personal grants from Fortum Foundation (number 201800142) and from the Finnish Foundation for Technology Promotion (number 6712).

Conflict of Interest

The authors declare no conflict of interest.

Keywords: hydrodeoxygenation · propylphenol · propylbenzene · reducible support · platinum

[1] S. H. Mohr, J. Wang, G. Ellem, J. Ward, D. Giurco, *Fuel* **2015**, *141*, 120–135.
[2] J. Clark, F. Deswarte, *Introduction to Chemicals from Biomass*, John Wiley & Sons Ltd, Sussex **2015**, p.344.
[3] S. N. Naik, V. V. Goud, P. K. Rout, A. K. Dalai, *Renewable Sustainable Energy Rev.* **2010**, *14*, 578–597.
[4] J. C. Serrano-Ruiz, J. A. Dumesic, *Energy Environ. Sci.* **2011**, *4*, 83–99.
[5] R. P. Anex, A. Aden, F. K. Kazi, J. Fortman, R. M. Swanson, M. M. Wright, J. A. Satrio, R. C. Brown, D. E. Daugaard, A. Platon, G. Kothandaraman, D. D. Hsu, A. Dutta, *Fuel* **2010**, *89*, S29–S35.
[6] J. P. Lange, *ChemSusChem* **2018**, *11*, 997–1014.
[7] J. Y. Kim, H. W. Lee, S. M. Lee, J. Jae, Y. K. Park, *Bioresour. Technol.* **2019**, *279*, 373–384.
[8] S. Xiu, A. Shahbazi, *Renewable Sustainable Energy Rev.* **2012**, *16*, 4406–4414.
[9] A. Gutierrez, E.-M. Turpeinen, T.-R. Viljava, O. Krause, *Catal. Today* **2017**, *285*, 125–134.
[10] A. V. Bridgwater, *Biomass Bioenergy* **2012**, *38*, 68–94.
[11] L. Fele Žilnik, A. Jazbinšek, *Sep. Purif. Technol.* **2012**, *86*, 157–170.
[12] H. Wang, J. Male, Y. Wang, *ACS Catal.* **2013**, *3*, 1047–1070.
[13] P. M. de Souza, R. C. Rabelo-Neto, L. E. P. Borges, G. Jacobs, B. H. Davis, T. Sooknoi, D. E. Resasco, F. B. Noronha, *ACS Catal.* **2015**, *5*, 1318–1329.
[14] A. M. Barrios, C. A. Teles, P. M. de Souza, R. C. Rabelo-Neto, G. Jacobs, B. H. Davis, L. E. P. Borges, F. B. Noronha, *Catal. Today* **2018**, *302*, 115–124.
[15] M. B. Griffin, G. A. Ferguson, D. A. Ruddy, M. J. Biddy, G. T. Beckham, J. A. Schaidle, *ACS Catal.* **2016**, *6*, 2715–2727.
[16] I. T. Ghampson, C. Sepúlveda, A. B. Dongil, G. Pecchi, R. García, J. L. G. Fierro, N. Escalona, *Catal. Sci. Technol.* **2016**, *6*, 7289–7306.
[17] A. N. Kay Lup, F. Abnisa, W. M. A. W. Daud, M. K. Aroua, *Appl. Catal. A* **2017**, *541*, 87–106.
[18] X. Zhang, J. Tang, Q. Zhang, Q. Liu, Y. Li, L. Chen, C. Wang, L. Ma, *Catal. Today* **2019**, *319*, 41–47.
[19] B. Feng, H. Kobayashi, H. Ohta, A. Fukuoka, *J. Mol. Catal. A* **2014**, *388–389*, 41–46.
[20] V. M. L. Whiffen, K. J. Smith, *Energy Fuels* **2010**, *24*, 4728–4737.
[21] H. Ohta, B. Feng, H. Kobayashi, K. Hara, A. Fukuoka, *Catal. Today* **2014**, *234*, 139–144.
[22] C. A. Teles, R. C. Rabelo-Neto, G. Jacobs, B. H. Davis, D. E. Resasco, F. B. Noronha, *ChemCatChem* **2017**, *9*, 2850–2863.
[23] D. Garcia-Pintos, J. Voss, A. D. Jensen, F. Studt, *J. Phys. Chem. C* **2016**, *120*, 18529–18537.
[24] Q. Sun, G. Chen, H. Wang, X. Liu, J. Han, Q. Ge, X. Zhu, *ChemCatChem* **2016**, *8*, 551–561.
[25] E. Kordouli, B. Pawelec, C. Kordulis, A. Lycourghiotis, J. L. G. Fierro, *Appl. Catal. B* **2018**, *238*, 147–160.
[26] H. Ohta, H. Kobayashi, K. Hara, A. Fukuoka, *Chem. Commun.* **2011**, *47*, 12209–12211.
[27] S. Velu, M. P. Kapoor, S. Inagaki, K. Suzuki, *Appl. Catal. A* **2003**, *245*, 317–331.
[28] M. S. Zanuttini, B. O. Dalla Costa, C. A. Querini, M. A. Peralta, *Appl. Catal. A* **2014**, *482*, 352–361.
[29] H. Wan, R. V. Chaudhari, B. Subramaniam, *Top. Catal.* **2012**, *55*, 129–139.
[30] J. He, C. Zhao, J. A. Lercher, *J. Catal.* **2014**, *309*, 362–375.
[31] M. Hellinger, H. W. P. de Carvalho, S. Baier, L. Gharnati, J.-D. Grunwaldt, *Chem. Ing. Tech.* **2015**, *87*, 1771–1780.
[32] H. Pourzolfaghar, F. Abnisa, W. M. A. Wan Daud, M. K. Aroua, *J. Anal. Appl. Pyrolysis* **2018**, *133*, 117–127.
[33] A. J. Foster, P. T. M. Do, R. F. Lobo, *Top. Catal.* **2012**, *55*, 118–128.
[34] S. K. Wu, P. C. Lai, Y. C. Lin, H. P. Wan, H. T. Lee, Y. H. Chang, *ACS Sustainable Chem. Eng.* **2013**, *1*, 349–358.
[35] H. Y. Zhao, D. Li, P. Bui, S. T. Oyama, *Appl. Catal. A* **2011**, *391*, 305–310.
[36] P. M. de Souza, R. C. Rabelo-Neto, L. E. P. Borges, G. Jacobs, B. H. Davis, D. E. Resasco, F. B. Noronha, *ACS Catal.* **2017**, *7*, 2058–2073.
[37] D. A. Ruddy, J. A. Schaidle, J. R. Ferrell III, J. Wang, L. Moens, J. E. Hensley, *Green Chem.* **2014**, *16*, 454–490.
[38] Z. Zheng, Z. Luo, C. Zhao, *ChemCatChem* **2018**, *10*, 1376–1384.
[39] R. C. Nelson, B. Baek, P. Ruiz, B. Goundie, A. Brooks, M. C. Wheeler, B. G. Frederick, L. C. Grabow, R. N. Austin, *ACS Catal.* **2015**, *5*, 6509–6523.

[40] K. L. Luska, P. Migowski, S. El Sayed, W. Leitner, *Angew. Chem.* **2015**, *127*, 15976–15981; *Angew. Chem. Int. Ed.* **2015**, *54*, 15750–15755.
[41] P. E. Ruiz, K. Leiva, R. Garcia, P. Reyes, J. L. G. Fierro, N. Escalona, *Appl. Catal. A* **2010**, *384*, 78–83.
[42] C. R. Lee, J. S. Yoon, Y. W. Suh, J. W. Choi, J. M. Ha, D. J. Suh, Y. K. Park, *Catal. Commun.* **2012**, *17*, 54–58.
[43] K. Leiva, C. Sepúlveda, R. García, J. L. G. Fierro, N. Escalona, *Catal. Commun.* **2014**, *53*, 33–37.
[44] H. Lee, H. Kim, M. J. Yu, C. H. Ko, J.-K. Jeon, J. Jae, S. H. Park, S.-C. Jung, Y.-K. Park, *Sci. Rep.* **2016**, *6*, 28765.
[45] H. Ohta, K. Tobayashi, A. Kuroo, M. Nakatsuka, H. Kobayashi, A. Fukuoka, G. Hamasaka, Y. Uozumi, H. Murayama, M. Tokunaga, M. Hayashi, *Chem. Eur. J.* **2019**, *25*, 14762–14766.
[46] Y. Zhang, P. Bi, J. Wang, P. Jiang, X. Wu, H. Xue, J. Liu, X. Zhou, Q. Li, *Appl. Energy* **2015**, *150*, 128–137.
[47] J. Zakzeski, P. C. A. Bruijnincx, A. L. Jongerius, B. M. Weckhuysen, *Chem. Rev.* **2010**, *110*, 3552–3599.
[48] C. Newman, X. Zhou, B. Goundie, I. T. Ghampson, R. A. Pollock, Z. Ross, M. C. Wheeler, R. W. Meulenberg, R. N. Austin, B. G. Frederick, *Appl. Catal. A* **2014**, *477*, 64–74.
[49] X. Xiao, H. Bergstrom, R. Saenger, B. Johnson, R. Sun, A. Peterson, *Catal. Sci. Technol.* **2018**, *8*, 1819–1827.
[50] S. M. Schimming, O. D. Lamont, M. König, A. K. Rogers, A. D. D'Amico, M. M. Yung, C. Sievers, *ChemSusChem* **2015**, *8*, 2073–2083.
[51] K. Kon, W. Onodera, S. Takakusagi, K. I. Shimizu, *Catal. Sci. Technol.* **2014**, *4*, 3705–3712.
[52] M. V. Cagnoli, A. M. Alvarez, N. G. Gallegos, J. F. Bengoa, C. D. D. de Souza, M. Schmal, S. G. Marchetti, *Appl. Catal. A* **2007**, *326*, 113–119.
[53] A. S. Bazhenov, M. M. Kauppinen, K. Honkala, *J. Phys. Chem. C* **2018**, *122*, 6774–6778.
[54] M. V. Ganduglia-Pirovano, A. Hofmann, J. Sauer, *Surf. Sci. Rep.* **2007**, *62*, 219–270.
[55] H. Y. T. Chen, G. Pacchioni, *ChemCatChem* **2016**, *8*, 2492–2499.
[56] M. Thommes, K. Kaneko, A. V. Neimark, J. P. Olivier, F. Rodriguez-Reinoso, J. Rouquerol, K. S. W. Sing, *Pure Appl. Chem.* **2015**, *87*, 1051–1069.
[57] C. Hernández Mejía, J. H. den Otter, J. L. Weber, K. P. de Jong, *Appl. Catal. A* **2017**, *548*, 143–149.
[58] K. A. Cychosz, R. Guillet-Nicolas, J. Garcia-Martinez, M. Thommes, *Chem. Soc. Rev.* **2017**, *46*, 389–414.
[59] S. J. Tauster, *Acc. Chem. Res.* **1987**, *20*, 389–394.
[60] G. Bergeret, P. Gallezot, *Handb. Heteregeneous Catal.* (Eds.: G. Ertl, H. Knözinger, F. Schuth, J. Weitkamp), WILEY-VHC Verlag GmbH & Co. KGaA, Weinheim **2008**, pp. 738–746.
[61] S. Li, Q. Xu, E. Uchaker, X. Cao, G. Cao, *CrystEngComm* **2016**, *18*, 2532–2540.
[62] A. V. Naumkin, A. Kraust-Vass, S. W. Gaarenstroom, C. J. Powell, *NIST X-ray Photoelectron Spectroscopy Database*, National Institute of Standards and Technology **2000**.
[63] I. Nowak, M. Ziolek, *Chem. Rev.* **1999**, *99*, 3603–3624.
[64] S. L. S. Kuś, M. Otremba, M. Taniewski, *Fuel* **2003**, *82*, 1331–1338.
[65] A. R. Puigdollers, P. Schlexer, S. Tosoni, G. Pacchioni, *ACS Catal.* **2017**, *7*, 6493–6513.
[66] D. A. G. Aranda, A. L. D. Ramos, F. B. Passos, M. Schmal, *Catal. Today* **1996**, *28*, 119–125.
[67] T. Huizinga, J. Van Grondelle, R. Prins, *Appl. Catal.* **1984**, *10*, 199–213.
[68] J. L. González Escobedo, E. Mäkelä, J. Neuvonen, P. Uusi-Kyyny, M. Lindblad, R. Karinen, R. L. Puurunen, *Adv. Sustain. Syst.* **2020**, DOI 10.1002/adsu.201900140, in press.
[69] J. W. Thybaut, M. Saeys, G. B. Marin, *Chem. Eng. J.* **2002**, *90*, 117–129.
[70] N. Yan, C. Zhao, P. J. Dyson, C. Wang, L. T. Liu, Y. Kou, *ChemSusChem* **2008**, *1*, 626–629.
[71] M. Y. Chen, Y. B. Huang, H. Pang, X. X. Liu, Y. Fu, *Green Chem.* **2015**, *17*, 1710–1717.
[72] H. Ohta, W. Kong, K. Yamamoto, M. Hayashi, *ChemistrySelect* **2017**, *2*, 4226–4229.
[73] H. Ohta, K. Yamamoto, M. Hayashi, G. Hamasaka, Y. Uozumi, Y. Watanabe, *Chem. Commun.* **2015**, *51*, 17000–17003.
[74] S. Brunauer, P. H. Emmett, E. Teller, *J. Am. Chem. Soc.* **1938**, *60*, 309–319.
[75] E. P. Barrett, L. G. Joyner, P. P. Halenda, *J. Am. Chem. Soc.* **1951**, *73*, 373–380.
[76] H. S. Fogler, *Elements of Chemical Reaction Engineering*, Pearson Education, Inc., Westford, Massachusetts, U. S. A. **2006**, pp 66–67.
[77] F. Kapteijn, J. Gascon, T. A. Nijhuis, *Catal. An Integr. Textb. Students* (Eds.: U. Hanefeld, L. Lefferts), Wiley-VCH Verlag GmbH & Co., Weinheim, Germany **2008**, pp. 221–271.
[78] J. T. Scanlon, D. E. Willis, *J. Chromatogr. Sci.* **1985**, *23*, 333–340.
[79] A. D. Jorgensen, K. C. Picel, V. C. Stamoudis, *Anal. Chem.* **1990**, *62*, 683–689.

Manuscript received: March 11, 2020
Revised manuscript received: May 16, 2020
Accepted manuscript online: May 20, 2020
Version of record online: June 30, 2020